Electronic Supplementary Material (ESI) for Inorganic Chemistry Frontiers.

Electronic Supplementary Information

Rationalization of TS-1 Synthesis through the Design of Experiments

Francesca Rosso, [a] Andrea Rizzetto, [a,b] Alessia Airi, [a] Khrystyna Khoma, [a,b] Matteo Signorile, [a] Valentina Crocellà, [a] Silvia Bordiga, [a] Simone Galliano, [a] Claudia Barolo, [a] Eugenio Alladio, *[a] and Francesca Bonino *[a]

[a] Department of Chemistry, NIS and INSTM Reference Centre, Università di Torino, Via G. Quarello 15, 10135 and Via P. Giuria 7, 10125, Torino, Italy.

[b] Department of Applied Sciences and Technology, Politecnico di Torino, Corso Duca degli Abruzzi 24, 10129, Torino, Italy (present address).

* Corresponding authors.

E-mail address: eugenio.alladio@unito.it (Eugenio Alladio), francesca.bonino@unito.it (Francesca Bonino)

Section S1. Synthesis of the TS-1 samples

Scheme S1. Direction of modification of the TS-1 catalyst, divided by aspect to improve.

Modification of the TS-1 synthesis		
Avoid coke formation	Avoid by-product formation	Enhance catalytic activity
Hierarchical TS-1 [1–3] Nanosized TS-1 [4,5] Hollow TS-1 [6,7]	Zn doping [8]	Au nanoparticle doping [9–11]

Scheme S1 reports a summary of the direction of modification of the TS-1 synthesis, beyond the optimization or control of the Ti coordination. Each column shows a drawback during the utilization of the TS-1 catalyst and the solution(s) explored by the researchers. The coke formation is the major responsible for the inactivation of the TS-1 (as in all zeolitic catalyst). It is due to difficulties in the diffusion of products outside the pore that causes multiple unwanted oxidation reactions. The multiple oxidation reactions lead to the formation of carbonaceous residues that block the zeolite pores. This could be avoided if the diffusion path of reagents and product is shortened. The hierarchization of the TS-1 zeolite, [1–3] the formation of nanosized TS-1 [4,5] and the formation of hollows inside the bulk zeolite [6,7] are the most important approaches used to overcome this problem.

An important feature of the TS-1 catalyst lies in its selectivity toward a particular partial oxidation product. In the case of the Hydrogen Peroxide (H_2O_2) to Propylene Oxide (HPPO) reaction, the Zn presence is reported to enhance the selectivity towards the propylene oxide over the by-products. [8]

Another interesting modification of the TS-1 catalyst consists in the doping with Au nanoparticles, for the *in situ* production of the H_2O_2 necessary as oxidating agent. [9–11]

Table S1. List of the conditions used for each synthesis. The conditions are slightly different from those suggested by the DoE due to pragmatic reasons. Lines N1-N9: syntheses belonging to the D-Optimal design. Line N10: centre point. Lines N11-N13: additional syntheses in the experimental domain, included in the model. Lines Ei-a: reproducibility samples synthesized before N1-N13 samples. Lines Ei-b: reproducibility samples synthesized after N1-N13 samples.

Name	t(H-TEOS) [1] (h)	t(H-TBOT) [2] (h)	T(H-TEOS) [3] (°C)	t(A) [4] (h)	T(A) [5] (°C)	t(Cry) [6] (h)	T(Cry) [7] (°C)
N1	4.25	24	25	24	25	23	110
N2	24	24	60	48	60	23	110
N3	26	4	60	24	25	167	110
N4	4	4	26	48	60	167	110
N5	4	4	60	48	25	22	170
N6	24.75	4	25	24	60	22	170
N7	4	26	24	48	60	22	170
N8	24	24	25	48	25	185	170
N9	4	24	60	24	60	185	170
N10	14	14	40	34.25	40	94	140
N11	4.25	4.25	23.5	48	25	167	110
N12	24	24	60	48	60	167	110
N13	4.5	24.5	40	49	40	23	170
E1-a	4.08	4.16	40	24.08	40	24	140
E2-a	4.33	4.33	40	24	40	24	140
E3-a	4.05	4	40	24	40	24	140
E1-b	4.05	4.5	40	24	40	23	140
E2-b	4.05	4.5	40	24	40	23	140
E3-b	4.05	4.5	40	23.9	40	23	140

[1] t(H-TEOS): TEOS hydrolysis time.

[2] t(H-TBOT): TEOT hydrolysis time.

[3] T(H-TEOS): TEOS hydrolysis temperature.

[4] t(A): aging time.

[5] T(A): aging temperature.

[6] t(Cry): crystallization time.

[7] T(Cry): crystallization temperature.

Section S2. Data manipulation to obtain the responses

Yield. The yield was calculated as follow:

$$\boldsymbol{Yield}\ (\%) = \frac{\boldsymbol{Mass\ of\ sample}\ (\boldsymbol{g})}{\boldsymbol{Calculated\ mass}\ (\boldsymbol{g})} * \mathbf{100}$$

Ti/Si*100. For each sample, four EDX spectra were recorded on as many large areas (spot size ca. 1000 μm^2). For each spectrum, the total Ti content was calculated as Ti/Si atomic percentage (Ti/Si*100); the four values were mediated and used as a response for the DoE.

LMCT onset. The reflectance spectra, in the range 200-400 nm, were vertically shifted to equalize them at 100% of reflectance at 400 nm. A horizontal line was tracked at 96% of reflectance, and the wavelength at the interception among the line and the curve was used as a response for the DoE (Figure S1). Figure S2 shows the DR-UV spectra of three TS-1 samples supplied by Evonik Industries, already studied by Signorile et al. [12,13]. The sample TS-1A was determined to contain only tetrahedral Ti sites; the samples TS-1B and TS-1C were found to contain defective Ti sites and TiO_2 respectively, in addition to a certain amount of tetrahedral Ti. Panel b shows the magnification of the region at high reflectance (%), to highlight the LMCT onset of these samples.

960 cm^{-1} area. The spectra were internally normalized at the band centred at 800 cm^{-1} (ascribed to the symmetric Si-O-Si stretching), as unaffected by the presence of Ti. They were then cut in the range 980-930 cm^{-1}, and the integrated area of this signal was used as a response for the DoE.

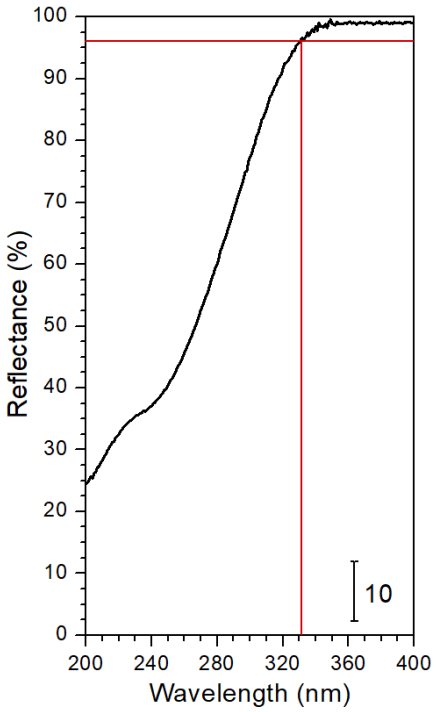

Figure S1. Schematic representation of the method used to determine the wavelength of the onset of the LMCT transition of Ti. The procedure was performed on the spectra in reflectance (%). The horizontal line is aligned at 96% of reflectance; the vertical line highlights the wavelength of the interception among the spectrum and the horizontal line.

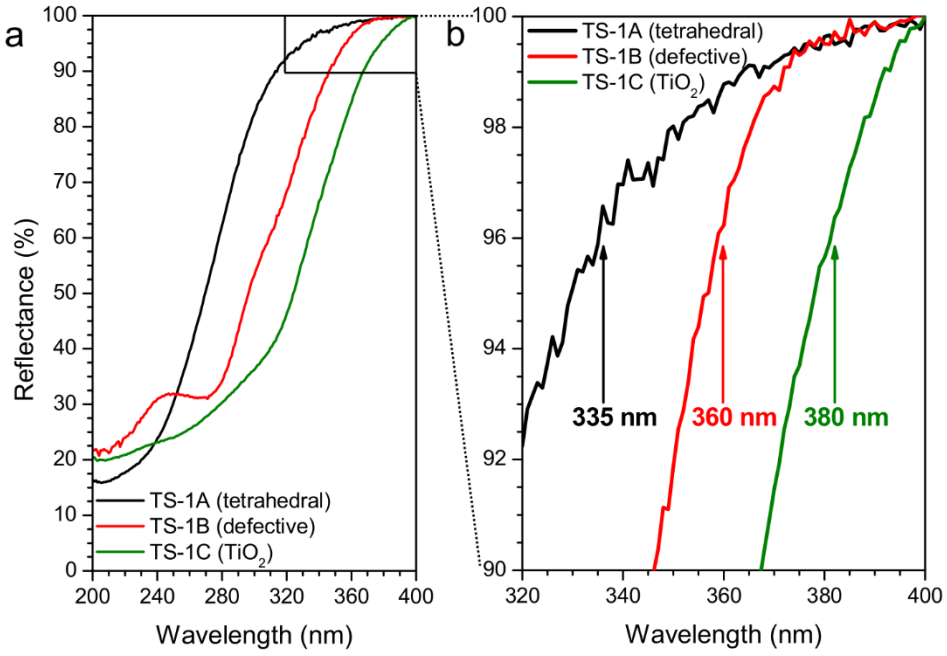

Figure S2. a) DR-UV spectra of the TS-1 samples, supplied by Evonik Industries, and in depth characterized and b) magnification of the range at high reflectance (%) to highlight the LMCT onset of the three samples.

Section S3. Reproducibility assessment

The reproducibility of the synthesis was tested to discern the effects that can be observed by varying the synthesis parameters from the unavoidable experimental variability. Figure S3 reports the XRD patterns (panel a), the DR-UV spectra (panel b) and the ATR-IR spectra (panel c) of the Ei-y series samples (produced for evaluating the reproducibility of the synthesis). Table S2 shows the corresponding responses. Only the Ei-b set of repetitions was included in the model for considering the experimental variability, since the inclusion of too many repeated points (not performed in the centre point, represented by the N10 sample) might alter the outcomes of the model.

Table S2. List of the responses obtained for each repeated synthesis. Lines Ei-a: reproducibility samples synthesized before N1-N13 samples. Lines Ei-b: reproducibility samples synthesized after N1- N13 samples.

Name	Yield (%)	Ti/Si*100 (mol/mol)	LMCT onset (nm)	960 cm^{-1} area (cm^{-1})
E1-a	75.35	0.95	340	0.216
E2-a	72.82	0.90	322	0.234
E3-a	74.40	0.86	316	0.263
E1-b	76.85	0.97	328	0.208
E2-b	77.06	0.85	330	0.196
E3-b	76.97	0.97	333	0.223

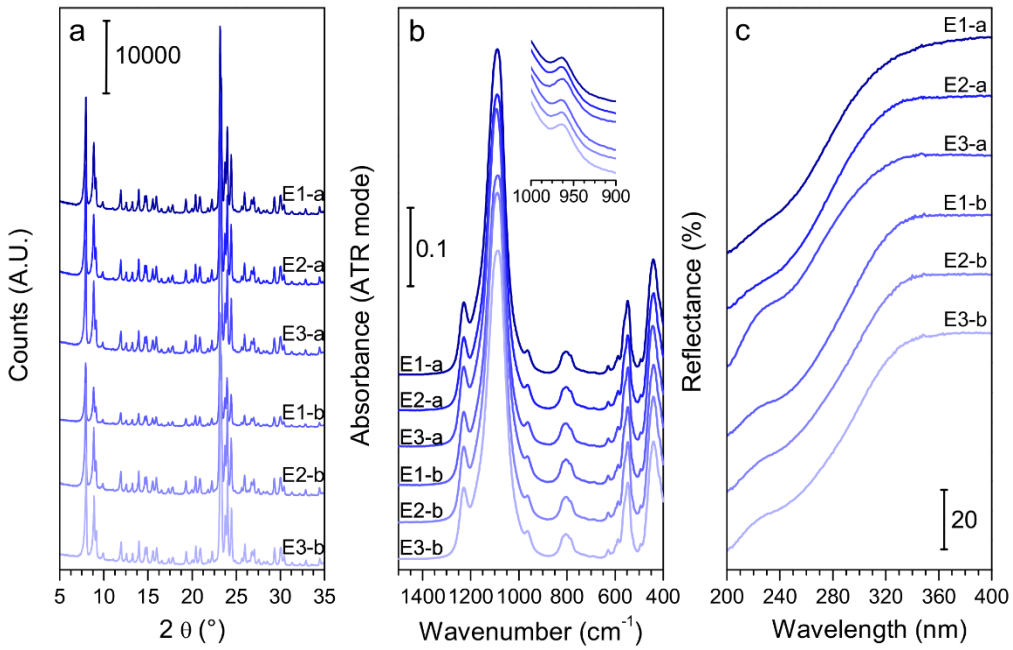

Figure S3. a) Diffraction patterns of the as synthesized reproducibility samples; b) ATR-IR spectra of the reproducibility samples; the inset reports the magnification of 960 cm^{-1} signal. c) DR-UV spectra of the activated reproducibility samples.

Section S3. Analysis of the responses through the DoE

Table S3 shows the centred and scaled coefficients with their absolute error, corresponding to half the error bar of the coefficient plots. The absolute error is calculated with a confidence level of 90%. The maximum and minimum possible levels of the responses (as calculated from the model) can be obtained by algebraic addition of the coefficients and their absolute error to obtain the predicted confidence intervals for the responses. Table S4 reports the maximum and minimum averages, the overall absolute error for the prediction of the response value, and the limits of the confidence intervals (at 90% of confidence level).

Table S3. Centred and scaled coefficients with their absolute error (calculated with a confidence level of 90%) for each response.

Response	Term	Coefficient	Absolute error
Yield (%)	Constant	78.78	3.54
	t(Cry)[1]	5.67	3.66
Ti/Si*100 (mol/mol)	Constant	1.27	0.15
	t(H-TBOT)[2]	0.17	0.15
	T(Cry)[3]	0.17	0.15
LMCT onset (nm)	Constant	340	7
	t(Cry)[1]	9	8
	T(Cry)[3]	9	8
960 cm^{-1} area (cm^{-1})	Constant	0.248	0.032
	T(Cry)[3]	0.054	0.033

[1] t(Cry): crystallization time.

[2] t(H-TBOT): TBOT hydrolysis time.

[3] T(Cry): crystallization temperature.

Table S4. Predicted average maximum, average minimum, absolute error and confidence interval (C. I.) for the maximum and minimum predicted levels of each response.

	Average max.	Average min.	Absolute error	C. I. (maximum)	C. I. (minimum)
Yield (%)	84.45	73.10	7.20	77.25 – 91.65	65.91 – 80.30
Ti/Si*100 (mol/mol)	1.61	0.92	0.45	1.16 – 2.06	0.47 – 1.38
LMCT onset (nm)	359	322	23	335 – 382	345 – 298
960 cm^{-1} area (cm^{-1})	0.302	0.194	0.064	0.238 – 0.367	0.130 – 0.258

Section S4. Evaluation of the responses by PCA

The reliability of the responses LMCT onset and 960 cm^{-1} area is evaluated through the PCA of the DR-UV and ATR-IR data, by comparison among the variability of the spectra (shown by the components obtained from the model) and the response. To graphically show the physical meaning of PC1, PC2 and PC3, spectra were reconstructed by multiplying the loadings of each PC by three arbitrary scores. In figure S2 and S3, the effect of PC1 is shown by multiplying the PC1 loadings by three demonstrative PC1 scores; the effects of PC2 and PC3 are shown by assigning a constant score to the PC1 (necessary to define the shape of the spectrum) and by choosing three demonstrative scores for PC2 and PC3 respectively. Consequently, the spectra reconstructed in Figure S2 and S3 represent some of the most interesting samples (out of those collected) according to their loadings values.

960 cm^{-1} area. The reconstructed spectra are reported in Figure S4a-c, to show the variability described by PC1 (a), PC2 (b) and PC3 (c). As it can also be deduced by Figure 4a-b, the variability among the spectra is mainly described by the PC2: a positive score for PC2 indicates that the samples have an elevated intensity of the 960 cm^{-1} signal, while a negative score for PC2 indicates that the samples have low intensity of the 960 cm^{-1} signal. Figure S4d shows the evident correlation among the response 960 cm^{-1} signal with PC2 and, consequently, the area of the 960 cm^{-1} signal, calculated as described in Section S2, represents the variability among the spectra.

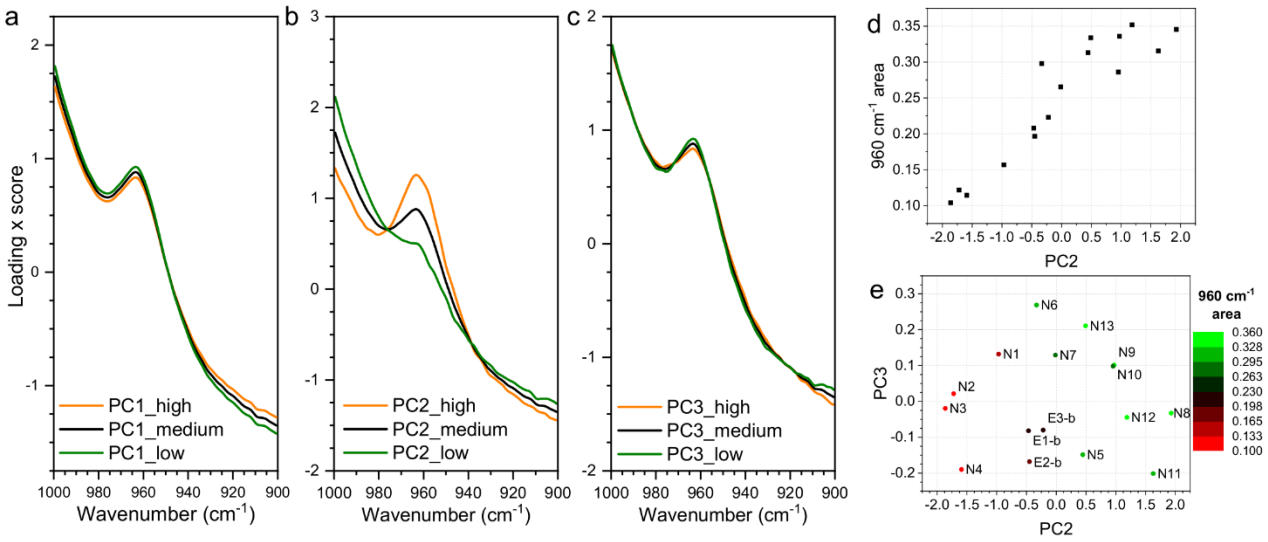

Figure S4. Reconstructed ATR-IR spectra in the range 1000-900 cm^{-1}, by assigning to the scores of PCs varying values (chosen coherently with the scores of the synthesized samples). (a) PC1 score = -9 (high), PC1 score = -9.5 (medium), PC1 score= -10 (low), PC2 score = 0 and PC3 score = 0. (b) PC1 score = -9.5, PC2 score = 2 (high), PC2 score = 0 (medium), PC2 score = -2 (low) and PC3 score = 0. (c) PC1 score = -9.5, PC2 score = 0, PC3 score = 0.3 (high), PC3 score = 0 (medium) and PC3 score = -0.3 (low). (d) 960 cm^{-1} area response as a function of PC2. (e) Scores plot of the PCA model developed on the ATR-IR data, colored by the 960 cm^{-1} area response.

LMCT onset. The reconstructed spectra are reported in Figure S5a-c, to show the variability described by PC1 (a), PC2 (b) and PC3 (c). The variability among the spectra described by the PC1 concerns the shape of the LMCT electronic transition involving Ti. The variability in the range 200-280 nm can be ascribed to the intensity of the LMCT transition, and the variability in the range 280-350 nm can be attributed to the light scattered differently by the samples. Since the spectra are recorded in reflectance (%) mode and, consequently, their intensity cannot be correlated with the species concentration, and since the study of the scattering is not the goal of this work, the variability among spectra described by PC1 is of little interest. The variability described by PC2 in the range 250-320 nm and by PC3 in the range 220-280 nm can be ascribed to the presence of amorphous species, instead. This result is coherent with the fact that the LMCT onset correlates mainly with PC2, but also partially with PC3 (Figure S5e) and, therefore, the LMCT onset response, as calculated in Section S2, well represents the variability among the spectra.

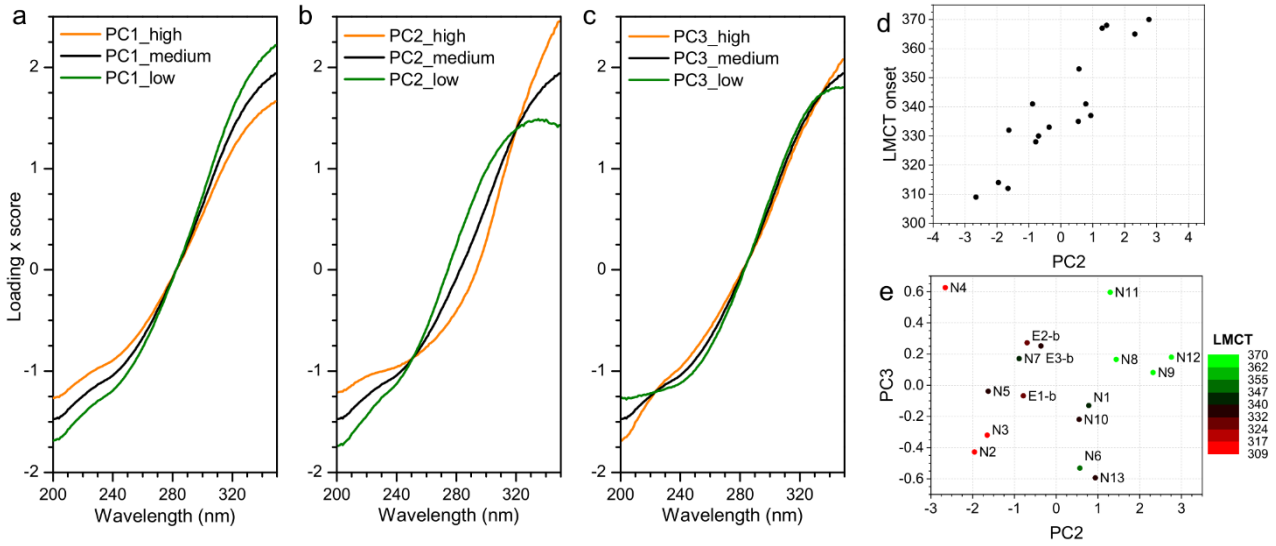

Figure S5. Reconstructed DR-UV spectra in the range 200-350 nm, by assigning to the scores of PCs varying values (chosen coherently with the scores of the synthesized samples). (a) PC1 score = -12 (high), PC1 score = -14 (medium), PC1 score = -16 (low), PC2 score = 0 and PC3 score = 0. (b) PC1 score = -14, PC2 score = 2 (high), PC2 score = 0 (medium), PC2 score = -2 (low) and PC3 score = 0. (c) PC1 score = -14, PC2 score = 0, PC3 score = 0.8 (high), PC3 score = 0 (medium) and PC3 score = -0.8 (low). (d) LMCT response as a function of PC2. (e) Scores plot of the PCA model developed on the DR-UV data, colored by the LMCT onset response.

References

1 M. Liu, J. Li, X. Chen, J. Song, W. Wei, Y. Wen and X. Wang, Preparation of anatase-free hierarchical titanosilicalite-1 in favor of allyl chloride epoxidation, *Microporous Mesoporous Mater.*, 2021, **326**, 111388.

2 Z. Wu, B. Wang, J. Shi, P. Rui, X. Xie, W. Liao and X. Shu, The silanization process for the hydrothermal synthesis of hierarchical titanium silicalite-1, *Microporous Mesoporous Mater.*, 2021, **327**, 111407.

3 M. Zhang, S. Ren, Q. Guo and B. Shen, Synthesis of hierarchically porous zeolite TS-1 with small crystal size and its performance of 1-hexene epoxidation reaction, *Microporous Mesoporous Mater.*, 2021, **326**, 111395.

4 H. Liu, Y. Wang, T. Ye, F. Wang, S. Ran, H. Xie, J. Liu, Y. Li, B. Li, Y. Liu, Y. Chai and L. Wang, Fully utilizing seeds solution for solvent-free synthesized nanosized TS-1 zeolites with efficient epoxidation of chloropropene, *J. Solid State Chem.*, 2022, **307**, 122844.

5 L. Zhang, X. Zhu, X. Wang and C. Shi, The synthesis of pure and uniform nanosized TS-1 crystals with a high titanium content and a high space-time yield, *Inorg. Chem. Front.*, 2021, **8**, 5260–5269.

6 Y. Liu, F. Wang, X. Zhang, Q. Zhang, Y. Zhai, G. Lv, M. Li and M. Li, One-step synthesis of anatase-free hollow titanium silicalite-1 by the solid-phase conversion method, *Microporous Mesoporous Mater.*, 2022, **331**, 111676.

7 M. Li, Y. Zhai, X. Zhang, F. Wang, G. Lv, A. Rosine, M. Li, Q. Zhang and Y. Liu, $(NH_4)_2SO_4$-assisted synthesis of thin-walled Ti-rich hollow titanium silicalite-1 zeolite for 1-hexene epoxidation, *Microporous Mesoporous Mater.*, 2022, **331**, 111655.

8 V. Arca, A. Boscolo Boscoletto, N. Fracasso, L. Meda and G. Ranghino, Epoxidation of propylene on Zn-treated TS-1 catalyst, *J. Mol. Catal. A Chem.*, 2006, **243**, 264–277.

9 Y. A. Kalvachev, T. Hayashi, S. Tsubota and M. Haruta, Vapor-phase selective oxidation of aliphatic hydrocarbons over gold deposited on mesoporous titanium silicates in the co-presence of oxygen and hydrogen, *J. Catal.*, 1999, **186**, 228–233.

10 T. A. Nijhuis, B. J. Huizinga, M. Makkee and J. A. Moulijn, Direct epoxidation of propene using gold dispersed on TS-1 and other titanium-containing supports, *Ind. Eng. Chem. Res.*, 1999, **38**, 884–891.

11 Z. Su, L. Gao, J. Gao and W. Ma, Effect of nickel promoter in Au/TS-1 catalysts for gas-phase propylene epoxidation, *J. Porous Mater.*, 2022, **29**, 143–152.

12 M. Signorile, V. Crocellà, A. Damin, B. Rossi, C. Lamberti, F. Bonino and S. Bordiga, Effect of Ti Speciation on Catalytic Performance of TS-1 in the Hydrogen Peroxide to Propylene Oxide Reaction, *J. Phys. Chem. C*, 2018, **122**, 9021–9034.

13 M. Signorile, L. Braglia, V. Crocellà, P. Torelli, E. Groppo, G. Ricchiardi, S. Bordiga and F. Bonino, Computational Assessment of Relative Sites Stabilities and Site-Specific Adsorptive Properties of Titanium Silicalite-1 *Angew. Chemie - Int. Ed.*, 2020, **59**, 18145–18150.